Cell Cycle Control and Environmental Response by Second Messenger Networks in *Caulobacter Crescentus*

Chunrui Xu
Genetics, Bioinformatics, and Computational Biology
Virginia Polytechnic Institute and State University
Blacksburg, VA

Bronson Weston
Genetics, Bioinformatics, and Computational Biology
Virginia Polytechnic Institute and State University
Blacksburg, VA

Yang Cao*
ycao@cs.vt.edu
Department of Computer Science
Virginia Polytechnic Institute and State University
Blacksburg, VA

ABSTRACT

Second messengers are intracellular molecules which respond to extracullular signalling molecules and trigger physiological changes. The cyclic di-GMP (c-di-GMP) is a ubiquitous second messenger which coordinates various aspects of growth and behavior of bacteria. Recent work has disclosed that another second messenger - alarmones guanosine tetraphosphate and guanosine pentaphosphate ((p)ppGpp) - has antagonistic roles against c-di-GMP in the cell cycle regulation network. Both c-di-GMP and (p)ppGpp have been verified to have important impact on functions of bacteria, including biofilm formation, transcription, virulence, and quorum sensing. Moreover, (p)ppGpp accumulates under starvation in bacteria, helping bacteria to survive in stressful conditions through regulating concentrations of relative substances and morphology. In this work, we propose a mathematical model to represent these second messengers, and analyze how the network regulates the cell cycle of *C. crescentus* and responds to certain environmental changes through a nitrogen-based phosphotransferase system (PTS^{Ntr}). Our mathematical model consists of 7 ODEs describing the dynamics of 7 significant molecules. The simulated behavior of c-di-GMP, ratio (p)ppGpp/GTP and PTS^{Ntr} are consistent with experiments. Additionally, our model provides reasonable predictions for how concerned molecules, such as cdG and PTS^{Ntr} enzymes, change under nitrogen changes, which have not been explored or measured yet.

CCS CONCEPTS

• **Computing methodologies**;

KEYWORDS

c-di-GMP, (p)ppGpp, *Caulobacter crescentus*, cell cycle, nitrogen starvation

*corresponding author

Woodstock '18, June 03–05, 2018, Woodstock, NY

ACM ISBN 978-1-4503-9999-9/18/06…$15.00
https://doi.org/10.1145/1122445.1122456

ACM Reference Format:
Chunrui Xu, Bronson Weston, and Yang Cao. 2018. Cell Cycle Control and Environmental Response by Second Messenger Networks in *Caulobacter Crescentus*. In *Woodstock '18: ACM Symposium on Neural Gaze Detection, June 03–05, 2018, Woodstock, NY*. ACM, New York, NY, USA, 12 pages. https://doi.org/10.1145/1122445.1122456

1 INTRODUCTION

The alphaproteobacterium *Caulobacter crescentus* living in oligotrophic aquatic environments is a model organism for understanding cell differentiation and regulation of prokaryotes. *C. crescentus* undergoes asymmetric cell division, yielding two distinct progeny cells (Fig. 1): a non-motile 'stalked' cell (st) enters the next cell cycle and initiates DNA replication immediately, while a motile 'swarmer' cell (sw) differentiates into a stalked cell given sufficient nutrients before re-entering the cell cycle [40]. The stalked cell develops a holdfast to attach to solid surfaces, whereas the swarmer cell develops a flagellum to search for nutrients in liquid environments. The asymmetric cell cycle, which affords *C. crescentus* a certain time to find more nutrients, makes it feasible to live in oligotrophic water [36].

Since the asymmetric cell division pattern plays an essential role in survival in oligotrophic environments for *C. crescentus* and understanding how the pattern is regulated provides an insight into life cycle of many bacteria with similar characteristic, many proteins, genes, and other molecules are involved in the asymmetric pattern have been reported [16, 36]. The synthesis and degradation of important proteins at specific time and location account for a significant part of the regulation network. As a DNA-binding response regulator, CtrA is at the center of the highly ordered proteins in *C. crescentus*. CtrA functions as a transcription factor, activating or repressing more than 100 genes involved in flagellum biogenesis, DNA replication and methylation, and cell division [24, 35]. As CtrA inhibits the initiation of DNA duplication, active CtrA must be eliminated during swarmer-to-stalker transition for the entry of cell division. There are two pathways to inactivate CtrA: proteolysis by ClpXP [41] and dephosphorylation.

Recent research [19, 41] has shown that the spatio-temporally regulated proteolysis of CtrA requires protease ClpXP and additional factors called adaptors in *C. crescentus*. The adaptor complex consists of CpdR, RcdA, PopA, and a ubiquitous second messenger cyclic di-GMP (cdG) (Fig. 2). ClpXP primed by unphosphorylated CpdR locates at the old pole (Fig. 1) and recruits the adaptor RcdA which interacts with PopA directly. However, PopA must be bound with cdG to adapt CtrA to the entire protease complex (Fig. 2),

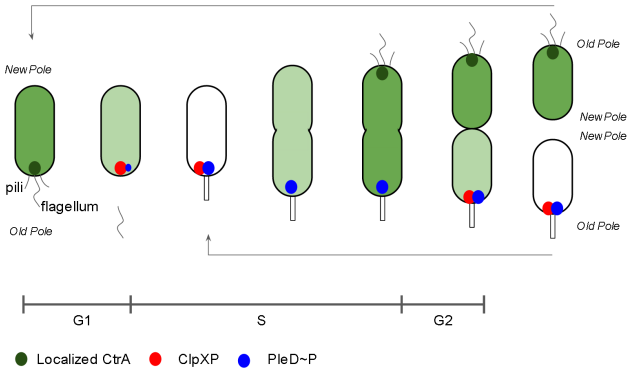

Figure 1: Asymmetric cell cycle and CtrA dynamics of *C. crescentus*. (1) Stalked cell is non-motile with a holdfast; Swarmer cell is motile with pill and flagellum, which transforms into a stalked cell before DNA replication. (2) CtrA regulates cell cycle of *C. crescentus* as a master regulator spatially and temporally. It is eliminated during G1-S transition which initiates DNA replication. The darker color indicates higher concentration. (3) ClpXP is the specific protease for CtrA, which shows up at specific location (old pole) to degrade CtrA. (4) PleD~P acts as the major synthetase of c-di-GMP at specific location (old pole).

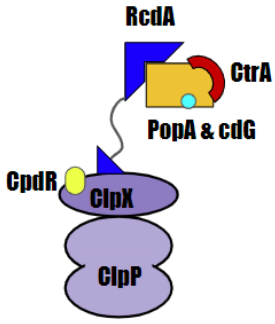

Figure 2: Model of the protease complex for CtrA in *C. crescentus*. Proteolysis of CtrA relies on protease ClpXP and additional adaptors. Only primed (by CpdR) ClpXP is able to recruit RcdA. RcdA tethers PopA and primed ClpXP. The second messenger c-di-GMP is required to adapt CtrA to the protease ClpXP.

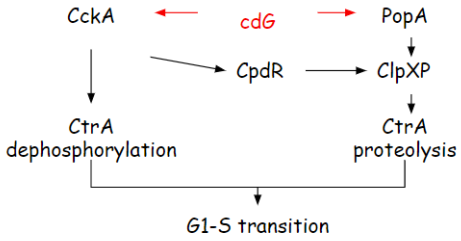

Figure 3: C-di-GMP regulates *C. crescentus* S-phase entry through CtrA in *C. crescentus*. (1) c-di-GMP directly stimulates phosphatase activity through binding CckA, thereby dephosphorylating CtrA to allow replication initiation. (2) c-di-GMP is required in proteolysis of CtrA.

which means cdG is indispensable for CtrA proteolysis. Besides working in CtrA proteolysis, c-di-GMP also participates in CtrA dephosporylation by stimulating the CckA phosphatase activity [27]. CckA is a bifunctional enzyme, which can act both as phosphoatase and kinase to regulate CtrA and CpdR. CdG directly binds to CckA to switch it from kinase to phosphatase activities during the G1-S transition, which stimulates the dephosphorylation of CtrA and CpdR rapidly. Then the DNA replication is initiated [6]. Therefore, c-di-GMP regulates both phosphorylation and stability of CtrA (Fig. 3) to stimulate entry into S-phase.

Compared with cdG, the hyperphosphorylated guanosine tetraphosphate (ppGpp) and guanosine pentaphosphate (pppGpp) have antagonistic functions to regulate the cell cycle. (p)ppGpp is converted into GTP in metabolism and uses GTP as the substrate during synthesis, which shares the common intermediate GTP with cdG. (p)ppGpp promotes the motile and non-replicative fates by inducing arrest of G1 phase [12]. The upshift of (p)ppGpp in *C. crescentus* increases CtrA levels as well. Therefore, the second messengers c-di-GMP and (p)ppGpp regulate CtrA through complementary mechanisms.

Additionally, the second messengers c-di-GMP and (p)ppGpp have been reported to control several key processes to help bacteria to adapt to various environmental factors [12, 20]. Exploring how environmental restriction affects cell cycle provides insight into why *C. crescentus* is able to live in oligotrophic environments. Therefore, the relationship between environment and second messengers is of great interest. Nutrients such as carbon and nitrogen have impacts on cdG as well as (p)ppGpp regulations. There are some evidences [12] showing that bacteria accumulate (p)ppGpp following stressful environmental changes by the RelA-SpoT homologue (RSH) family of bifunctional enzymes. Also, bacteria respond to the availability of carbon through cdG regulated signaling processes [20]. However, the specific mechanism of how stressful conditions affect cell cycle through the second messenger networks and other key proteins in *C. crescentus* is not very clear.

In this work, we combine the network involving regulations of c-d-GMP, (p)ppGpp, and GTP into one mathematical model to investigate how second messenger networks control the asymmetric cell cycle pattern and respond to environmental change in *C. crescentus* through a phosphotransferase system (PTS). The important enzymes responsible for synthesis and hydrolysis of cdG and (p)ppGpp are included. Our simulation shows that c-di-GMP decreases dramatically following nitrogen deprivation, which suggests one possible mechanism for bacteria responding to nitrogen starvation. As cdG plays an important role in dephosphorylation and proteolysis of CtrA, which is one of the master regulators involved in cell cycle, our model relates the environmental changes with cell cycle quantitatively. The specific levels of several significant molecules in bacteria such as (p)ppGpp, GTP, and PTS enzymes

have not been measured yet experimentally. Our model is able to provide predicted concentrations for these variables under high nitrogen and starved condition in bacteria.

2 METHODS

.

2.1 Diagram Construction

In order to explain how cdG and (p)ppGpp regulate cell cycle and respond to environment, it is necessary to construct a complete diagram including cdG, (p)ppGpp, and the bridge connecting environment with (p)ppGpp - PTS^{Ntr} system. We investigated the metabolism of cdG and (p)ppGpp in *C. crescentus*, and found GTP is one important intermediate connecting these two second messengers. Enzymes within PTS^{Ntr} regulate the synthesis and degradation of (p)ppGpp.

2.1.1 Metabolism and Characterization of c-di-GMP. c-di-GMP controls the transition between a motile cell and a sessile cell in *C. crescentus*. Two kinds of antagonistic enzymes, diguanylate cyclases (DGCs) and phosphodiesterases (PDEs), regulate the cellular concentration of cdG [17](Fig. 4). The synthases DGCs like PleD and DgcB, whose activities reside in the highly conserved GGDEF domain, act as dimers to produce cdG from two molecules of GTPs [39]. The I-site of DGCs can be bound by cdG to inhibit the synthetase activity, which is known as the product inhibition (Fig. 4).

The hydrolases PDEs, such as PdeA and PdeB, cleave cdG to pGpG or GMP based on the conversed EAL domain or HD-GYP domain [39]. As pGpG is eventually converted into GMP (Fig. 4), we ignored pGpG and used GMP as the product of cdG degradation. In addition, the activity of some EAL domains in *C. crescentus* is activated by GTP through binding GTP in the non-active GGDEF domain of PDEs [7]. The velocity of PDE reaches $V_{max}/2$ when concentration of GTP is 4μM. We ignored this activation in our model because the estimated levels of GTP in some bacteria is much larger than 4μM.

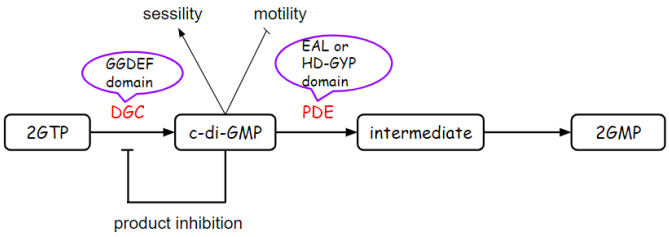

Figure 4: A schematic that shows metabolism of c-di-GMP. The synthase cyclases (DGCs) catalyse the synthesis of cdG through the catalytic GGDEF domains. Specific phosphodiesterases (PDEs) make use of EAL or HD-GYP domains to cleave cdG into pGpG (an intermediate which is subsequently turned into GMP) or GMP. Product inhibition indicates that cdG binds to the I-site of DGCs and inhibits the synthetase activity.

2.1.2 Metabolism and Characterization of (p)ppGpp. (p)ppGpp plays important roles in several processes, including transcription, translation, and DNA replication [20]. It accumulates in most bacteria during stress, starvation, and entry in stationary phase. The abrupt environmental changes associated with the (p)ppGpp accumulation are provoked by the intracellular increase [15] of GTP/GDP (Fig. 5). (p)ppGpp alerts bacteria to nutrient deprivation through modifying the physiology. In *C. crescentus*, (p)ppGpp delays the entry into S phase to prolong the G1 phase, and maintains the flagellum organelle in G1 phase. That helps *C. crescentus* to survive in nutrient-deprived environments by delaying DNA replication, which gives bacteria more time to search for food in the environment.

C. crescentus utilizes a RelA homologue (SpoT), which acts as the key bifunctional enzyme [13] to synthesize and degrade (p)ppGpp (Fig. 5). The bifunctional enzyme SpoT uses ATP and GTP/GDP to generate (p)ppGpp, and is responsible for degrading (p)ppGpp to GDP/GTP as well. SpoT regulates (p)ppGpp through two distinct active sites within two separate domains, which are regulated by a reciprocal mechanism coupled with opposing states ((p)ppGpp-hydrolase-OFF/synthase-ON and hydrolase-ON/synthase-OFF) [15].

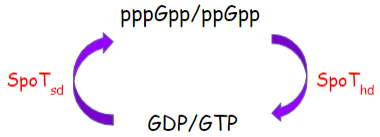

Figure 5: Metabolism of (p)ppGpp. SpoT in *C. crescentus* catalyzes both the synthesis and hydrolysis of (p)ppGpp. ATP and P_i are not shown.

GTP and GMP are the source and eventual product of cdG, respectively (Fig. 4). As GTP/GDP also plays a role as source and product in mechanism of (p)ppGpp (Fig. 5), we can easily use GTP as the bridge to connect two essential second messengers - cdG and (p)ppGpp - into one diagram. The second messenger networks including (p)ppGpp and c-di-GMP have been summarized in Fig. 6 [5]. As GMP, GDP, and GTP can be converted to each other in one mechanism circle and biologists usually mention ppGpp and pppGpp together [13, 15, 20], we combine GDP with GTP as one variable.

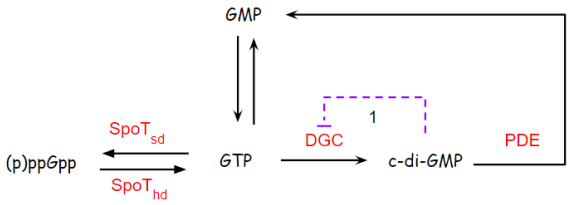

Figure 6: Diagram of second messenger networks. GTP connects the second messengers (p)ppGpp and cdG because it is an intermediate in the metabolisms of these two second messengers. $SpoT_{sd}$ and $SpoT_{hd}$ represent the synthase activity and hydrolase activity of bifunctional enzyme SpoT. The metabolism cycle for GTP/GMP is simplified through combining GDP with GTP as one variable. (1) Dashed line 1 indicates the production inhibition based on cdG binding I-site of DGCs. (2) Dashed line 2 indicates the inhibition from (p)ppGpp on the synthase of GTP [13].

2.1.3 Nutrient-related Phosphotransferase System (PTS). It has been well documented that (p)ppGpp responds to carbon and nitrogen deprivation. While the specific mechanism underlying carbon starvation is not clear yet, the mechanism responsible for nitrogen starvation has been recently elucidated [12]. (p)ppGpp accumulates following nitrogen starvation, which affords bacteria to regulate cellular processes such as DNA replication, transcription and translation [34]. The mechanism regulating (p)ppGpp concentration is based on the nitrogen-related phosphoenolpyruvate (PEP) phosphotransferase system (PTS^{Ntr}) [13, 34].

The PTS^{Ntr} system consists of three types of phosphorylation components (EI^{Ntr}, NPr, and $EIIA^{Ntr}$) which form a phosphorylation cascade (Fig. 7). The first protein EI^{Ntr} initiates the cascade through autophosphorylation using PEP as the phosphoryl donor. Then the phosphoryl group is transferred from EI^{Ntr} to NPr and then to $EIIA^{Ntr}$. $EIIA^{Ntr}$ acts as a reversible phosphate sink or transfers phosphoryl group to other unknown molecules [32].

PTS^{Ntr} regulates the SpoT activity, which decides the level of (p)ppGpp (Fig. 5), through receiving intracellular glutamine to affect (p)ppGpp. Genome of *C. crescentus* suggests that the assimilation of inorganic nitrogen is tightly dependent on the glutamine synthetase activity. Therefore, glutamine acts as a nitrogen signal which is transduced from PTS^{Ntr} to (p)ppGpp to regulate the cell cycle progression [10, 34]. Glutamine binds to the conserved GAF domain of EI^{Ntr} to inhibit its autophosphorylation. Therefore, enzymes involved in PTS^{Ntr} become highly phosphorylated under nitrogen starvation when the intracellular level of glutamine decreases rapidly [12]. Bacterial two-hybrid (BTH) assays [34] have shown that phosphorylated $EIIA^{Ntr}$ directly interacts with SpoT whereas phosphorylated NPr controls the SpoT activity indirectly. Mutant experiments further indicate that $EIIA^{Ntr}$~P inhibits hydrolase activity (HD) of SpoT, whereas NPr~P regulates control SpoT synthase activity (SD) indirectly.

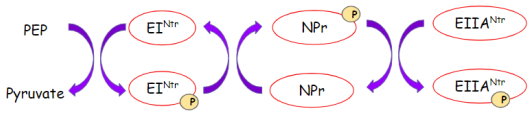

Figure 7: The phosphorylation cascade in nitrogen-related phosphotransferase system (PTS^{Ntr}). PTS^{Ntr} consists of three phosphorylation components (EI^{Ntr}, NPr, and $EIIA^{Ntr}$) which responds to nitrogen availability. Phosphoenolpyruvate (PEP) performs as the phosphoryl donor in the phosphorylation cascade.

Summarizing the aforementioned relationships, PTS^{Ntr} connects glutamine which acts as the nitrogen signal with the bifunctional enzyme SpoT which switches (p)ppGpp and GTP back and forth. Therefore, we involved PTS^{Ntr} in our second messenger network to extend the model with environmental change (Fig. 8).

2.2 Mathematical Model

Based on the diagram in Fig. 8, the simplified reactions for our model are as following:

The diguanylate cyclases (DGCs) activity is contained within dimers, where each GGDEF domain is loaded with one GTP molecule [29]. Additionally, the activity of DGCs is subject to product

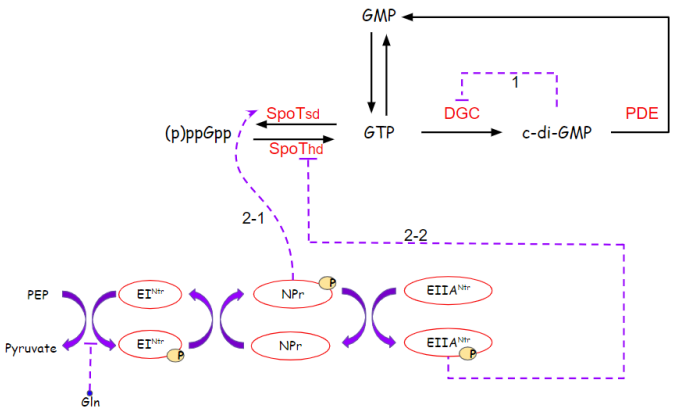

Figure 8: Diagram of our second messenger model. Glutamine (Gln) acts as the nitrogen signal, which regulates the phosphorylated state of enzymes within PTS^{Ntr}. (1) Dashed line 3-1 indicates phosphorylated NPr activates indirectly the synthase activity of SpoT. (2) Dashed line 3-2 indicates phosphorylated $EIIA^{Ntr}$ inhibits directly the hydrolase activity of SpoT.

inhibition through binding of cdG to the I-site. Here we assumed that this reaction is cooperative binding and used 2 as the Hill exponent to describe the cooperativity of product inhibition (Table 1, Equation 1). As PleD is the major DGC in *C.crescentus* and another synthetase DgcB is expressed throughout the cell cycle [2], we used PleD with a basal level of DGC to represent DGCs. Unlike DGCs, phosphodiesterases (PDEs) act as monomers, which convert cdG to GMP eventually. As PdeA acts as the major PDE in in *C.crescentus*, we used PdeA to represent PDEs in Table 1 Equation 1.

$$2\,\mathrm{GTP} \xrightarrow{\mathrm{DGC}} \text{c-di-GMP},$$
$$\text{c-di-GMP} \xrightarrow{\mathrm{PDE}} 2\mathrm{GMP}\,.$$

The synthase activity (sd) and hydrolase activity (hd) of bifunctional enzyme SpoT catalyze the reaction between (p)ppGpp and GTP. Taking the activation and inhibition from NPr and phosphorylated $EIIA^{Ntr}$ into consideration, we used the Michaelis-Menten equation to describe the direct and indirect interaction with unknown mechanism (Table 1, Equation 2) [37]. $SpoT_{sd}$ and $SpoT_{hd}$ in Equation 2 indicates the proportion of synthase and hydrolase in total SpoT, respectively.

$$(\mathrm{p})\mathrm{ppGpp} \underset{\mathrm{SpoT(sd)}}{\overset{\mathrm{SpoT(hd)}}{\rightleftharpoons}} \mathrm{GTP}.$$

The metabolism of GTP/GMP is regulated through reversible reactions, where we combined GDP with GTP as one variable.

$$\mathrm{GTP} \rightleftharpoons \mathrm{GMP}.$$

PEP binds to the C-terminal domain of EI and donates a phosphoryl group to the site of His-189 (Fig. 9). Then the phosphoryl group is transferred to the next two enzymes - NPr and EIIA [43, 45]. The phosphorylation cascade is summarized as the following reactions.

$$\mathrm{EI} + \mathrm{PEP} \underset{k_{b_{-1}}}{\overset{k_{b_1}}{\rightleftharpoons}} \mathrm{EI}^{\mathrm{PEP}},$$

$$\mathrm{EI}^{\mathrm{PEP}} \underset{k_{-1}}{\overset{k_1(\text{inhibited by Gln})}{\rightleftharpoons}} \mathrm{EI}\sim\mathrm{P}^{\mathrm{Pyr}},$$

$$\mathrm{EI}\sim\mathrm{P}^{\mathrm{Pyr}} \underset{k_{b_2}}{\overset{k_{b_{-2}}}{\rightleftharpoons}} \mathrm{EI}\sim\mathrm{P} + \mathrm{Pyr},$$

$$\mathrm{EI}\sim\mathrm{P} + \mathrm{NPr} \underset{k_{-2}}{\overset{k_2}{\rightleftharpoons}} \mathrm{EI} + \mathrm{NPr}\sim\mathrm{P},$$

$$\mathrm{NPr}\sim\mathrm{P} + \mathrm{EIIA} \underset{k_{-3}}{\overset{k_3}{\rightleftharpoons}} \mathrm{NPr} + \mathrm{EIIA}\sim\mathrm{P}\cdot$$

$\mathrm{EI}^{\mathrm{PEP}}$ and $\mathrm{EI}\sim\mathrm{P}^{\mathrm{Pyr}}$ indicate EI bound with PEP and EI~P bound with Pyr, respectively. $k_{\pm i}$ $(i = 1, 2, 3)$ represents the rates of phosphorylation reactions, while $k_{b_{\pm j}}$ $(j = 1, 2)$ represent the rates of binding reactions. Glutamine binds to $\mathrm{EI}^{\mathrm{PEP}}$ to inhibit its phosphorylation.

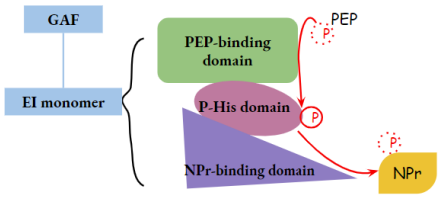

Figure 9: Schematic diagram of EI structure and phosphate transfer. The C-terminus of EI bears a PEP-binding domain and the N-terminus is responsible for binding NPr. The red arrow indicates the direction of phosphate transfer. The separate GAF domain interacting with Glutamine is responsible for receiving the nitrogen signal.

In the PTS reactions, binding of PEP is a quite rapid process which has been verified in fluorescence spectroscopy studies [21]. Here, we make several assumptions to describe $\mathrm{PTS}^{\mathrm{Ntr}}$ reactions effectively:
(1). We assume that PEP and Pyr binding reactions are much faster than phosphorylation (reaching quasi steady state). Therefore, we converted the binding reactions into algebraic equations (Tabel 1, Equation 8,9).
(2). As Glutamine (Gln) binds to the GAF domain of $\mathrm{EI}^{\mathrm{Ntr}}$, which is a separate domain of EI [31] (Fig. 9), we assume that the binding of Gln is allosteric inhibition (Tabel 1, Equation 5).
(3). There is limited numeric data for $\mathrm{PTS}^{\mathrm{Ntr}}$. As enzymes within $\mathrm{PTS}^{\mathrm{Ntr}}$ are homologs with enzymes within PTS, we introduced some numeric data from PTS into our model, including reaction rates and concentration constants.
(4). The total concentrations of $\mathrm{EI}^{\mathrm{Ntr}}$, NPr and $\mathrm{EIIA}^{\mathrm{Ntr}}$ are assumed to be constants as shown in [44]: $[\mathrm{EI}^{\mathrm{Ntr}}]_{\mathrm{tot}} = 10\mu\mathrm{M}$, $[\mathrm{NPr}]_{\mathrm{tot}} = 50\mu\mathrm{M}$, and $[\mathrm{EIIA}^{\mathrm{Ntr}}]_{\mathrm{tot}} = 50\mu\mathrm{M}$ (Tabel 1, Equation 10, 11, 12).
(5). According to previous experiments [14] in *Escherichia coli*, we set the concentrations of PEP and pyruvate to 2.8mM and 0.9mM in starvation, while 0.3mM and 1.5mM in abundant nitrogen.

Eventually, we obtain a system with 7 ODEs and 5 algebraic equations in Table 1. More details are shown in Supplementary Materials A.1. Parameters are explained in details in Table 2. Parameters in our model (Table 2) were taken or estimated from experimental observations when it is possible, or estimated based on data fitting with the maximum point of experimental cdG [1]. Initial conditions in Table 3 were estimated from the intracellular concentrations of bacteria. We adjusted the corresponding initial conditions keeping the same magnitude with experiments. The maximum concentration of cdG in Caulobacter is around 2.8μM [1]. Basal level of (p)ppGpp in gram-negative bacteria during normal condition is around 10μM [9]. The ratio of (p)ppGpp/GTP [3, 4] was used to estimate the initial conditions of GTP and GMP. Equations were solved with ode15s in Matlab.

3 SIMULATION AND RESULTS

As mentioned in previous simulation [26], the total time of cell cycle in our simulation is also set as 150 min.

3.1 Simulation of DGCs and PDEs

As PleD and PdeA are the major DGCs and PDEs in *Caulobacter Crescentus*, we simulated PleD and PdeA with curve fitting tool in Matlab as two periodical functions to estimate intracellular levels of DGCs and PDEs. We plug these two functions into our mathematical model to describe the levels of DGCs and PDEs quantitatively. Besides PleD, there are other DGCs in bacteria participating in making cdG[2, 38]. Abel et al[2] indicates that DgcB, which is expressed throughout the cell cycle, cooperates with PleD for cdG synthesis. Therefore, we add a basal level of DGCs in Table 1, Equation 1.

Since reliable data on active PleD (phosphorylated) level over the cell cycle were not available in literature (Supplementary materials A.2), we borrowed the results of an, as of yet, unpublished model by Bronson Weston which is more consistent with qualitative experimental information (Fig. 1). Weston's simulation and the corresponding periodical function are shown in Fig. 10a. R-square of PleD fit is 0.98. We quantitatively extracted PdeA concentration from Joshi et al's Western blots [18] using ImageJ. The quantitative PdeA points and the corresponding fitting curve are shown in Fig. 10b. R-square of PdeA fit is 0.78.

3.2 Simulations under starvation and nitrogen-rich condition

Goodwin et al's [11] experiments reveal how glutamine inhibits kinetics of $\mathrm{EI}^{\mathrm{Ntr}}$ quantitatively with concentration of glutamine being 0, 10, 100, and 1000 μ M. Here, we used Gln=100μM to represent nitrogen starvation and Gln=1000μM to describe abundant nitrogen in environment to verify the feasibility of our mathematical model. From Hogema et al's experiments [14], we set PEP=300μM and Pyr=1500μM under rich nutrients condition; PEP=2800μM and Pyr=900μM under starved condition. In addition, we simulated *Caulobacter* following Gln=1000μM, PEP=2800μM, Pyr=900μM and Gln=100μM, PEP=300μM, Pyr=1500μM to analyze how glutamine and PEP/Pyr impact variables (Fig. 11, Fig. 12). In order to fit Goodwin et al's experimental observation well in [11], we used $\frac{K_4+\epsilon[\mathrm{Gln}]}{K_4+[\mathrm{Gln}]}$ to describe this inhibition in Table 1 Equation 5, where parameters were estimated from [11] as well.

Fig. 11 and Fig. 12 compare the changes of important variables under different conditions. Fig. 11(a) and (c) represent simulations under nitrogen rich and starvation, respectively. (b) and (d) are plot to provide single-variable comparison. In Fig. 11, cdG shows a stable

Table 1: Equations of our mathematical model.

$$\frac{d[\text{cdG}]}{dt} = \text{k}_{\text{s.cdG}} \times [\text{PleD+basal DGC}] \times \frac{K_1^2}{K_1^2+[\text{cdG}]^2} \times \frac{[\text{GTP}]^2}{[\text{GTP}]^2+K_{\text{m1}}^2} - k_{\text{d.cdG}} \times [\text{PdeA}] \times \frac{[cdG]}{[cdG]+K_{\text{m2}}} (1)$$

$$\frac{d[(\text{p})\text{ppGpp}]}{dt} = \text{k}_{\text{s.(p)ppGpp}} \times \text{SpoT}_{\text{sd}}^{*} \times \frac{[\text{GTP}]}{[\text{GTP}]+K_{\text{m3}}} - k_{\text{d.(p)ppGpp}} \times \text{SpoT}_{\text{hd}}^{*} \times \frac{[(\text{p})\text{ppGpp}]}{[(\text{p})\text{ppGpp}]+K_{\text{m4}}} (2)$$

$$\frac{d[\text{GTP}]}{dt} = \text{k}_{\text{s.GTP}} \times [\text{GMP}] - k_{\text{d.GTP}} \times [\text{GTP}] - \frac{d(p)ppGpp}{dt} - 2k_{\text{s.cdG}} \times [\text{PleD+basal DGC}] \times \frac{K_1^2}{K_1^2+[\text{cdG}]^2} \times \frac{[\text{GTP}]^2}{[\text{GTP}]^2+K_{\text{m1}}^2} (3)$$

$$\frac{d[\text{GMP}]}{dt} = 2\text{k}_{\text{d.cdG}} \times [\text{PdeA}] \times \frac{[cdG]}{[cdG]+K_{\text{m2}}} + k_{\text{d.GTP}} \times [\text{GTP}] - k_{\text{s.GTP}} \times [\text{GMP}] (4)$$

$$\frac{d[\text{EI~P}]_{\text{tot}}}{dt} = \text{k}_1 \times \frac{K_4+\epsilon[\text{Gln}]}{K_4+[\text{Gln}]} \times [\text{EI}^{\text{PEP}}] - k_{-1}[\text{EI~P}^{\text{Pyr}}] - k_2[\text{EI~P}][\text{NPr}] + k_{-2}[\text{NPr~P}][\text{EI}] (5)$$

$$\frac{d[\text{NPr~P}]}{dt} = \text{k}_2[\text{EI~P}][\text{NPr}] - k_{-2}[\text{NPr~P}][\text{EI}] - (k_3[\text{NPr~P}][\text{EIIA}] - k_{-3}[\text{NPr}][\text{EIIA~P}]) (6)$$

$$\frac{d[\text{EIIA~P}]}{dt} = \text{k}_3[\text{NPr~P}][\text{EIIA}] - k_{-3}[\text{NPr}][\text{EIIA~P}] - k_{\text{d.EIIA}}[\text{EIIA~P}] (7)$$

$$[\text{EI}][\text{PEP}] = \text{K}_{b_1}^{*}[\text{EI}^{\text{PEP}}] (8)$$

$$[\text{EI~P}][\text{Pyr}] = \text{K}_{b_2}^{*}[\text{EI~P}^{\text{Pyr}}] (9)$$

$$[\text{EI}]_{\text{tot}} = [\text{EI}]+[\text{EI}^{\text{PEP}}]+[\text{EI~P}^{\text{Pyr}}]+[\text{EI~P}] (10)$$

$$[\text{NPr}]_{\text{tot}} = [\text{NPr}]+[\text{NPr~P}] (11)$$

$$[\text{EIIA}]_{\text{tot}} = [\text{EIIA}]+[\text{EIIA~P}] (12)$$

* $\text{SpoT}_{sd} = \frac{\alpha}{1+\alpha}$, $SpoT_{hd} = \frac{1}{1+\alpha}$, $\alpha = \text{K}_{\text{SpoT}} \times \frac{[\text{NPr~P}]}{[\text{NPr~P}]+\text{K}_2} / \frac{\text{K}_3}{[\text{EIIA~P}]+\text{K}_3}$

$K_{b_1} = \frac{k_{b_{-1}}}{k_{b_1}}$, $K_{b_2} = \frac{k_{b_{-2}}}{k_{b_2}}$

All enzyme-involved inhibition and activation items are indicated by Hill equations or Michaelis-Menten equations.

In order to improve the efficiency and decrease the complexity of modelling, we used hybrid modelling approach to describe reactions [5].

oscillation under nutrient-rich condition. cdG decreases dramatically under starvation whereas (p)ppGpp increases dramatically. Comparing (a) with (b) and (d), decrease of Gln and increase of ratio PEP/Pyr from 300/1500 to 2800/900 can both amplify reduction of cdG and accumulation of (p)ppGpp. In Fig. 12, all three enzymes become highly phosphorylated under nitrogen starvation.

4 DISCUSSION

4.1 Concentration and Oscillation of c-di-GMP over cell cycle in *C. crescentus*

C-di-GMP level oscillates during the cell cycle [1, 27], which plays an important role in cell cycle regulation and cell fate determination. We used one point of Abel et al's data to estimate unknown parameters and showed the comparison between our simulation and Abel et al's experiment in Fig. 13. Our simulation fits the experimental data reasonably well and shows a stable oscillation during cell cycle at high Gln concentration.

Abel et al's data peaks at the transition of swarmer-to-stalked cell (275nM) and then decreases until reaching the lowest value (<100nM) in the sw phase after cell division. Our simulation shows the highest level of cdG reaches at around 0.28 μM, and cdG decreases below 0.1 μM in swarmer cell, which is consistent with observations. We calculated the relative errors of each experimental point in Table 4. Except for these points with pretty low concentration, our simulation shows reasonable trends at correct time periods. However, both Table 4 and Fig. 13 display a few differences between simulation and observation points during late S-phage.

We summarized three potential reasons for these differences: (1) The concentration of phosphorylated PleD was from Weston's model, which is not completely finished. There may be some differences between Weston's simulation and vivo level of PleD. (2) The western blots of PdeA and measure of cdG may include some errors experimentally. It is hard to measure the intracellular concentration precisely especially considering that cdG keeps a very low level during late S-phage. (3) Althought PleD and PdeA are the major synthase and hydrolase of cdG respectively, other DGC and PDE enzymes[38] like DgcC and PdeB need to be considered more.

4.2 Concentrations of Concerned Molecules and Important Ration

There is no specific experimental data of GTP and (p)ppGpp levels in *C. crescentus*. However, the ratio ppGpp/GTP changes from around 0.1 under carbon-rich condition to 1.5 following glucose starvation in *C. crescentus* [4]. Krol et al's work has shown that ppGpp increases more under nitrogen starvation than carbon starvation in *Sinorhizobium meliloti* [22]. From Fig. 11, our simulation shows that the ratio (p)ppGpp/GTP changed from around 0.1 under nitrogen-rich condition (Fig. 11(a)) to 2.3 under starvation (Fig. 11(c)), which was reasonable compared with existing information. (p)ppGpp did increase obviously following nitrogen deprivation in our simulation,

Table 2: Parameters.

parameter	description	source
$k_{\text{s.cdG}} = 0.6/min$	synthesis rate constant of cdG	data fitting
$k_{\text{d,cdG}} = 1.15/min$	degradation rate constant of cdG	estimated from [7]
$\text{K}_1 = 0.55\mu M$	dissociation constant for product inhibition	[33]
K_{m1}=100μ M	binding affinity of GTP	data fitting
$K_{\text{m2}} = 0.06\mu M$	binding affinity of cdG	[33]
basal DGC=0.11μM	basal DGCs activity except PleD	data fitting
Periodical functions of PleD and PdeA	enzyme activity	Bronson Weston's model and [18]
$k_{\text{s.(p)ppGpp}} = 600/min$	scaled synthesis rate of (p)ppGpp	data fitting
$k_{\text{d.(p)ppGpp}} = 350/min$	scaled degradation rate of (p)ppGpp	data fitting
$K_2 = 600\mu M$	binding affinity of NPr~P	data fitting
$K_3 = 800\mu M$	dissociation constant of EIIA~P	data fitting
$K_{\text{m3}} = 30\mu M$	binding affinity of GTP	data fitting
$K_{\text{m4}} = 100\mu M$	binding affinity of (p)ppGpp	[25]
$K_4 = 108\mu M$ $\epsilon = 0.17$	parameters of glutamine inhibition	[11]
$k_{\text{s.GTP}} = 800/min$	scaled synthesis rate of GTP	data fitting
$k_{\text{d.GTP}} = 1000/min$	scaled degradation rate of GTP	data fitting
$[\text{EI}]_{tot} = 10\mu M$ $[\text{NPr}]_{tot} = 50\mu M$ $[\text{EIIA}]_{tot} = 50\mu M$	total enzymes levels	[44]
$k_1 = 8.856 \times 10^6/h$ $k_{-1} = 11.21 \times 10^6/h$ $k_{\pm 2} = 2.95 \times 10^8/h$ $k_{\pm 3} = 9 \times 10^7/h$	phosphotransfer constants	[28, 44, 45]
$K_{\text{b1}} = 0.35$ $K_{\text{b2}} = 0.67$	binding constants	[45]

Table 3: Initial Conditions.

Variables	Initial Conditions (μM)
c-di-GMP	0.25
GTP	100
(p)ppGpp	5
GMP	60
EI~P	5
NPr~P	50
EIIA~P	50

Table 4: Relative Error of cdG simulation.

Time Period (min)	$\text{RE}_{\text{accuracy}}$ (%)
35-40	55
50-55	11
62	1
75-90	57
102	95
122	95
142	94

which had been proved experimentally in *C. crescentus*. Considering Fig. 11(b)(d), our simulation shows that decrease of glutamine and change of PEP and Pyr (from PEP=300μM, Pyr=1500μM to PEP=2800μM, Pyr=900μM) both decrease c-di-GMP and increase (p)ppGpp, which provide a potential explanation for how Gln and PEP/Pyr affect cell cycle.

Enzymes within the nitrogen-related phosphotransferase system (PTS^{Ntr}) became highly phosphorylated under glutamine starvation in Fig. 12, which was consistent with the existing qualitative analysis as well [12]. In addition, our simulation shows the ratio PEP/Pyr varying from 1/5 to 28/9 increases phosphorylated NPr and phosphorylated EIIA^{Ntr} but decreases phosphorylated EI^{Ntr}.

There are several points obtained from our simulation results which need to be verified in experiments further:

(1) The simulated GTP, GMP, and (p)ppGpp reach their steady states at specific levels quickly (Fig. 11). Therefore, the exact levels of GTP, GMP, and (p)ppGpp under eutrophic and starved conditions need to be measured by experiments to understand the mechanism of (p)ppGpp in details.

(2) Qualitative changes of PTS^{Ntr} enzymes have been ensured in previous researches. However, what are the specific levels of phosphorylated enzymes following starvation is of interest. The concentrations of phosphorylated PTS^{Ntr} enzymes did increase obviously under starvation in our simulation. The exact levels and changes of PTS enzymes need to be measured in wet experiments.

(3) The level of cdG decreases dramatically following starvation in our simulation, but it still oscillates a little bit (Fig. 11(b)). We

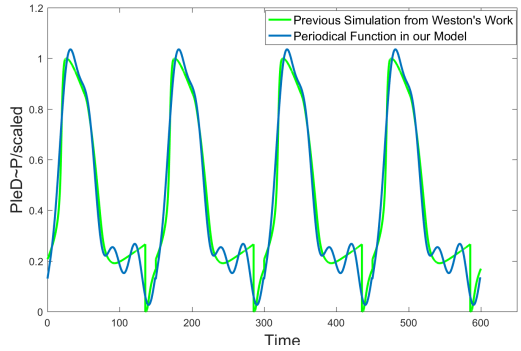

(a) Fitting curve of phosphorylated PleD.

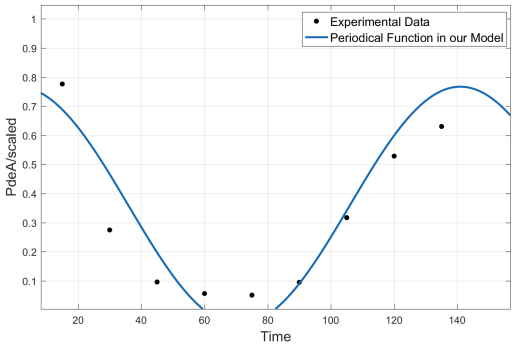

(b) Fitting curve of PdeA.

Figure 10: Periodical Functions of PleD and PdeA Used in the Mathematical Model. (a) Fitting function of PleD is the summation of sine functions: $5.175\times\sin(0.0009292\times t+0.005578)+0.2046\times\sin(0.07623\times t-1.11)+0.6235\times\sin(0.03333\times t+0.4149)+0.06622\times\sin(0.1963\times t-3.666)$. Negative values in PleD are replaced by 0. (*b*) Fitting function of PdeA is sine function: $0.4085\times\sin(\pi\times t/70+7.811)+0.3586$. The negative values in PdeA are replaced by 0. Experimental data were extracted from Joshi et al's western blot [18].

suspected that oscillation because oscillations would likely go away under cell cycle arrest. The decrease of cdG under starvation could support the observations about increased (p)ppGpp and decreased CtrA at that condition. The increase of (p)ppGpp likely results in a decrease of cdG through GTP in our networks. Additionally, cdG helps proteolysis of CtrA. That gave us a possible mechanism underlying responses of (p)ppGpp and CtrA to nitrogen signal. Further wet experiments are required to explore how concentration of cdG changes under starvation.

4.3 Response to Environmental Change

Fig. 14 shows how *C. crescentus* responds to environmental nitrogen changes in simulation. The response time for starvation is within one cycle, which means *C. crescentus* can respond to nitrogen deprivation quickly. It also recovers quite quickly when we reset glutamine and PEP/Pyr to the initial values. That would be a useful

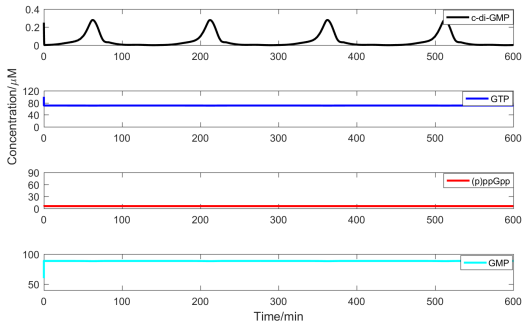

(a) Gln=1000μM, PEP=300μM, and Pyr=1500μM.

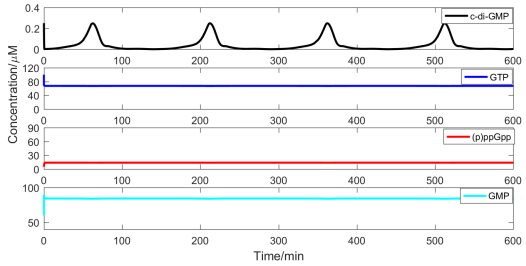

(b) Gln=100μM, PEP=300μM, and Pyr=1500μM.

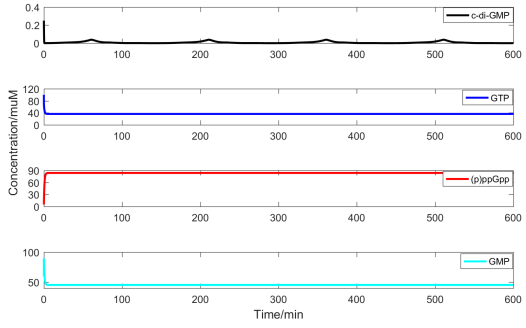

(c) Gln=100μM, PEP=2800μM, and Pyr=900μM.

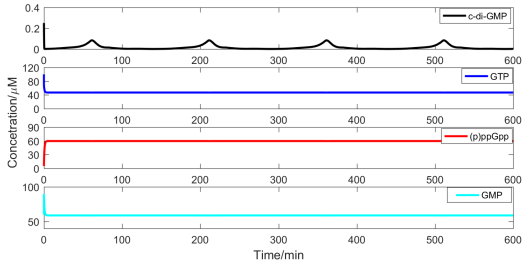

(d) Gln=1000μM, PEP=2800μM, and Pyr=900μM.

Figure 11: Simulations of c-di-GMP, GTP, (p)ppGpp, and GMP. Gln=1000μM indicates abundant nitrogen in environment, whereas Gln=100μM indicates nitrogen deprivation.

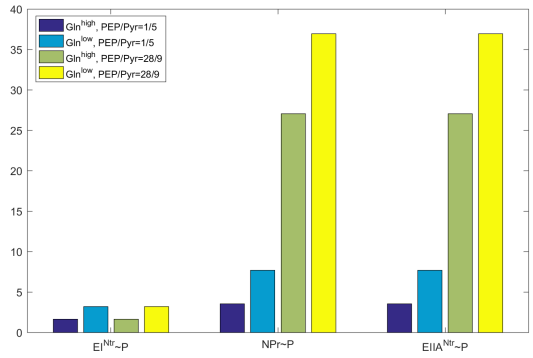

Figure 12: Simulations of Enzymes (EI^{Ntr}~P, NPr~P, and $EIIA^{Ntr}$~P) within PTS^{Ntr}. Gln^{high} indicates Gln=1000μM, and Gln^{low} indicates Gln=100μM. PEP/Pyr=1/5 shows the ratio of PEP/Pyr under PEP=300μM and Pyr=1500μM. PEP/Pyr=28/9 shows the ratio of PEP/Pyr under PEP=2800μM and Pyr=900μM.

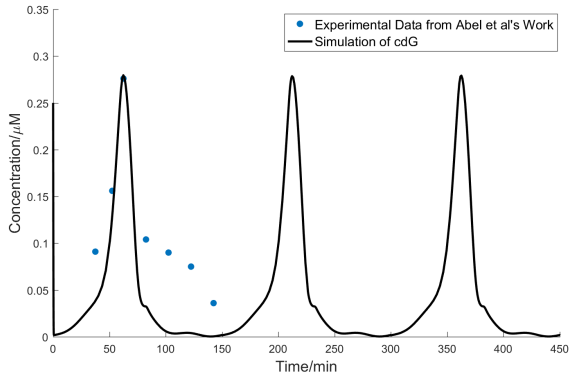

Figure 13: C-di-GMP oscillates during cell cycle. Blue dots indicate experimental data of c-di-GMP oscillation in a single *C. crescentus* wild type cell during one cell cycle [1]. Only c-di-GMP of swarmer cell is shown. Black line indicates the simulation result of c-di-GMP generated from our model (at Gln=1000μM, PEP=0.3Mm, and Pyr=1.5mM). We tracked the dynamics of c-di-GMP in swarmer cell only as well.

characteristic for *C. crescentus* to exist in oligotrophic environments. Additionally, the simulated steady state levels of GTP and (p)ppGpp do keep the same values as shown in Fig. 11, showing the stability of the simulation system.

4.4 Fitting PTS^{Ntr} separately to the experimental data

PTS and PTS^{Ntr} have a lot in common. Enzymes within PTS^{Ntr} (EI^{Ntr}, NPr, and $EIIA^{Ntr}$) are homologs of enzymes within PTS (EI, HPr, and EIIA/B/C). They have similar structures and play parallel roles in nutrients uptake. In addition, both systems are able to communicate with each other by phosphate exchange[8, 31].

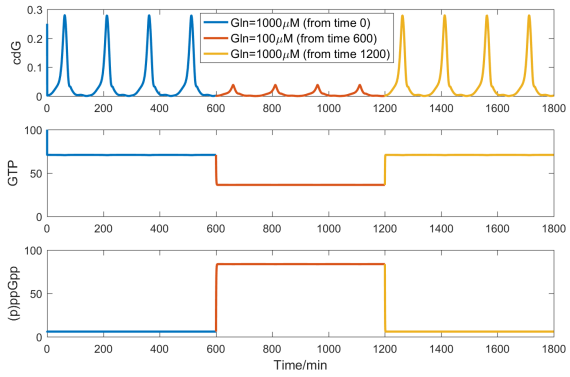

Figure 14: Response to nitrogen source changes in *C. crescentus*. Blue line indicates simulated levels of cdG, GTP, and (p)ppGpp when Gln=1000μM. Red line indicates simulated levels of these three molecules when glutamine changes to 100μM at simulation time 600. Yellow line indicates the simulation when the glutamine recovers to 1000*mu*M. The end points of previous simulation is used to be the initial point of the next simulation at a different glutamine level.

There are two significant differences between these two systems: (1). Enzymes II in PTS help nutrient transmembrane transport whereas $EIIA^{Ntr}$ do not. (2). PTS^{Ntr} can accept the glutamine signal. We plot Figure 7 based on the forementioned facts.

However, there is limited numeric data for PTS^{Ntr} in publications. Based on the similarities between PTS^{Ntr} and PTS, we introduced some parameters obtained from PTS experiments to simulate PTS^{Ntr} [44, 45] (Tabel 2). In order to verify how the PTS^{Ntr} model works, we set Gln to 0 and compare simulations with PTS experiments.

Kundig and Roseman[23, 43] have measured how EI and HPr level affect phosphorylation degree quantitatively (Table 5, Table 6). We introduced given conditions and simulated the corresponding phosphorylation degree. There is no information of Pyr in their experiments. We estimated concentration of Pyr based on one set of experimental data (Table 5). Relative errors shown in Table 5 and Table 6 indicate our PTS model can fit Kundig et al's experimental data well.

Table 5: Effect of EI level on the phosphorylation

Conditions: T=37°C, pH=7.4, PEP=160μM, HPr=24.4μM			
EI (nM)	EI~P+HPr~P (μM)	simulated* EI~P+HPr~P (μM)	$RE_{accuracy}$ (%)
15	6	6.9	15
312.5	6.5	7	8
729	7	7.2	3
1570	7.5	7.5	-**

* Pyr=620μM in simulation, which was estimated from the experimental data in the last row.
**The last row has been used to estimate Pyr level.

Table 6: Effect of HPr level on the phosphorylation

Conditions: T=37°C, pH=7.4, PEP=160μM, Pyr=620μM, EI=729nM			
HPr (μM)	EI~P+HPr~P (μM)	simulated* EI~P+HPr~P (μM)	$RE_{accuracy}$ (%)
0	>0*	0.32	-
10.5	3	3.34	11
21	5.85	6.36	9
31.5	9.1	9.37	3

* Too small to recognize specific value from the original figure[23].

4.5 The Mathematical Model and Future Work

Our mathematical model of second messengers for cell cycle regulations in *Caulobacter* (Fig. 8) summarize the current knowledge compiled from the literature. Most previous research has focused separately on mechanism of the cdG [1, 7] or the PTS system [11, 12] in bacteria, but has never related second messenger networks with the PTS system to study the impacts of environmental signals. Additionally, comprehensive mathematical exploration is limited.

In this work, the interactions within the second messenger network are converted into a set of differential equations and algebraic equations (Table 1) to simulate second messengers quantitatively. The current model consists of 7 ODEs and 5 algebraic equations, representing the synthesis, degradation, activation, inhibition, phosphorylation, dephosphorylation, binding, and release of physiological variables within *C.crescentus*. Although the comparisons between simulation results and experimental results taken from certain literature look good and encouraging, there are a few aspects can be considered in the future:

(1) As more experimental observations are developed, goodness of fitting for DGCs and PDEs can be improved. The parameter estimation will have more reference data as well.

(2) Involving the second messengers model into the big regulatory picture of cell cycle in *C.crescentus* will provide more insight into regulation mechanism and environmental response of bacteria. The resulted mathematical model will be inevitablely big and will involve different reaction scales. However, that will be a natural extension from our current models.

(3) This model can only simulate temporal dynamics of related variables, but both c-di-GMP and (p)ppGpp regulate cell cycle and morphological development temporally and spatially. Therefore, considering the localization factors into the second messengers model will contribute more in understanding cell cycle mechanism.

(4) The parameters sensitivity analysis can be further done to test the robustness of our mathematical model.

(5) The concentration of PEP and Pyr are set to specific values at specific nitrogen condition in our simulation. PEP and Pyr can be considered as variables as well to explore the specific mechanisms underlying receiving nutrient signals.

Overall, the work presented here is just the first step towards the modeling of second messenger network that involves cells' interaction with environmental change. More detailed models and analysis are expected to appear in our future work.

ACKNOWLEDGMENTS

This work was partially supported by the National Science Foundation under awards CCF-0953590, CCF-1526666, and MCB-1613741.

REFERENCES

[1] Sören Abel, Tabitha Bucher, Micaël Nicollier, Isabelle Hug, Volkhard Kaever, Pia Abel Zur Wiesch, and Urs Jenal. 2013. Bi-modal Distribution of the Second Messenger c-di-GMP Controls Cell Fate and Asymmetry during the Caulobacter Cell Cycle. *PLOS GENETICS* 9, 9 (SEP 2013). https://doi.org/{10.1371/journal.pgen.1003744}

[2] SÃűren Abel, Peter Chien, Paul Wassmann, Tilman Schirmer, Volkhard Kaever, MichaelÂăT. Laub, TaniaÂăA. Baker, and Urs Jenal. 2011. Regulatory Cohesion of Cell Cycle and Cell Differentiation through Interlinked Phosphorylation and Second Messenger Networks. *Molecular Cell* 43, 4 (2011), 550 – 560. https://doi.org/10.1016/j.molcel.2011.07.018

[3] Camille Benoist, Cyprien Guérin, Philippe Noirot, and Etienne Dervyn. 2015. Constitutive Stringent Response Restores Viability of *Bacillus subtilis* Lacking Structural Maintenance of Chromosome Protein. *PLOS ONE* 10, 11 (NOV 5 2015). https://doi.org/{10.1371/journal.pone.0142308}

[4] Cara C. Boutte, Jonathan T. Henry, and Sean Crosson. 2012. ppGpp and Polyphosphate Modulate Cell Cycle Progression in *Caulobacter crescentus*. *JOURNAL OF BACTERIOLOGY* 194, 1 (JAN 2012), 28–35. https://doi.org/{10.1128/JB.05932-11}

[5] Sascha Bulik, Sergio Grimbs, Carola Huthmacher, Joachim Selbig, and Hermann G. Holzhütter. 2009. Kinetic hybrid models composed of mechanistic and simplified enzymatic rate laws - a promising method for speeding up the kinetic modelling of complex metabolic networks. *FEBS JOURNAL* 276, 2 (JAN 2009), 410–424. https://doi.org/{10.1111/j.1742-4658.2008.06784.x}

[6] Y. Erin Chen, Christos G. Tsokos, Emanuele G. Biondi, Barrett S. Perchuk, and Michael T. Laub. 2009. Dynamics of Two Phosphorelays Controlling Cell Cycle Progression in *Caulobacter crescentus*. *JOURNAL OF BACTERIOLOGY* 191, 24 (DEC 15 2009), 7417–7429. https://doi.org/{10.1128/JB.00992-09}

[7] Matthias Christen, Beat Christen, Marc Folcher, Alexandra Schauerte, and Urs Jenal. 2005. Identification and characterization of a cyclic di-GMP-specific phosphodiesterase and its allosteric control by GTP. *JOURNAL OF BIOLOGICAL CHEMISTRY* 280, 35 (SEP 2 2005), 30829–30837. https://doi.org/{10.1074/jbc.M504429200}

[8] Fabian M Commichau, Karl Forchhammer, and JÃűrg StÃijlke. 2006. Regulatory links between carbon and nitrogen metabolism. *Current Opinion in Microbiology* 9, 2 (2006), 167 – 172. https://doi.org/10.1016/j.mib.2006.01.001 Cell Regulation / Edited by Werner Goebel and Stephen Lory.

[9] Rebecca M. Corrigan, Lauren E. Bellows, Alison Wood, and Angelika Gründling. 2016. ppGpp negatively impacts ribosome assembly affecting growth and antimicrobial tolerance in Gram-positive bacteria. *Proceedings of the National Academy of Sciences* 113, 12 (2016), E1710–E1719. https://doi.org/10.1073/pnas.1522179113 arXiv:https://www.pnas.org/content/113/12/E1710.full.pdf

[10] Bert Ely, ABC Amarasinghe, and Robert A Bender. 1978. Ammonia Assimilation and Glutamate Formation in *Caulobacter crescentus*. *JOURNAL OF BACTERIOLOGY* 133, 1 (1978), 225–230.

[11] Reed A. Goodwin and Daniel J. Gage. 2014. Biochemical Characterization of a Nitrogen-Type Phosphotransferase System Reveals that Enzyme EI^{Ntr} Integrates Carbon and Nitrogen Signaling in *Sinorhizobium meliloti*. *JOURNAL OF BACTERIOLOGY* 196, 10 (MAY 2014), 1901–1907. https://doi.org/{10.1128/JB.01489-14}

[12] Régis Hallez, Marie Delaby, Stefano Sanselicio, and Patrick H. Viollier. 2017. Hit the right spots: cell cycle control by phosphorylated guanosines in alphaproteobacteria. *NATURE REVIEWS MICROBIOLOGY* 15, 3 (MAR 2017), 137–148. https://doi.org/{10.1038/nrmicro.2016.183}

[13] Vasili Hauryliuk, Gemma C. Atkinson, Katsuhiko S. Murakami, Tanel Tenson, and Kenn Gerdes. 2015. Recent functional insights into the role of (p)ppGpp in bacterial physiology. *NATURE REVIEWS MICROBIOLOGY* 13, 5 (MAY 2015), 298–309. https://doi.org/{10.1038/nrmicro3448}

[14] Boris M. Hogema, Jos C. Arents, Rechien Bader, Kevin Eijkemans, Hiromi Yoshida, Hideyuki Takahashi, Hiroji Alba, and Pieter W. Postma. 1998. Inducer exclusion in *Escherichia coli* by non-PTS substrates: the role of the PEP to pyruvate ratio in determining the phosphorylation state of enzyme IIA^{Glc}. *MOLECULAR MICROBIOLOGY* 30, 3 (NOV 1998), 487–498. https://doi.org/{10.1046/j.1365-2958.1998.01053.x}

[15] Tanis Hogg, Undine Mechold, Horst Malke, Mike Cashel, and Rolf Hilgenfeld. 2004. Conformational antagonism between opposing active sites in a bifunctional RelA/SpoT homolog modulates (p)ppGpp metabolism during the stringent response (vol 177, pg 57, 2004). *CELL* 117, 3 (APR 30 2004), 415. https://doi.org/{10.1016/S0092-8674(04)00406-4}

[16] Urs Jenal. 2009. The role of proteolysis in the *Caulobacter crescentus* cell cycle and development. *RESEARCH IN MICROBIOLOGY* 160, 9 (NOV 2009), 687–695. https://doi.org/{10.1016/j.resmic.2009.09.006}

[17] Urs Jenal and Jacob Malone. 2006. Mechanisms of cyclic-di-GMP signaling in bacteria. *ANNUAL REVIEW OF GENETICS* 40 (2006), 385–407. https://doi.org/{10.1146/annurev.genet.40.110405.090423}

[18] Kamal Kishore Joshi, Christine M. Battle, and Peter Chien. 2018. Polar Localization Hub Protein PopZ Restrains Adaptor-Dependent ClpXP Proteolysis in *Caulobacter crescentus*. *JOURNAL OF BACTERIOLOGY* 200, 20 (OCT 2018). https://doi.org/{10.1128/JB.00221-18}

[19] Kamal Kishore Joshi, Matthieu Bergé, Sunish Kumar Radhakrishnan, Patrick Henri Viollier, and Peter Chien. 2015. An Adaptor Hierarchy Regulates Proteolysis during a Bacterial Cell Cycle. *CELL* 163, 2 (OCT 8 2015), 419–431. https://doi.org/{10.1016/j.cell.2015.09.030}

[20] Dimpy Kalia, Gökce Merey, Shizuka Nakayama, Yue Zheng, Jie Zhou, Yiling Luo, Min Guo, Benjamin T. Roembke, and Herman O. Sintim. 2013. Nucleotide, c-di-GMP, c-di-AMP, cGMP, cAMP, (p)ppGpp signaling in bacteria and implications in pathogenesis. *CHEMICAL SOCIETY REVIEWS* 42, 1 (2013), 305–341. https://doi.org/{10.1039/c2cs35206k}

[21] Tatiana A. Karelina, Hongwu Ma, Igor Goryanin, and Oleg V. Demin. 2011. EI of the Phosphotransferase System of *Escherichia coli*: Mathematical Modeling Approach to Analysis of Its Kinetic Properties. *Journal of Biophysics* (Mar 20 2011). https://doi.org/{10.1155/2011/579402}

[22] Elizaveta Krol and Anke Becker. 2011. ppGpp in Sinorhizobium meliloti: biosynthesis in response to sudden nutritional downshifts and modulation of the transcriptome. *MOLECULAR MICROBIOLOGY* 81, 5 (SEP 2011), 1233–1254. https://doi.org/{10.1111/j.1365-2958.2011.07752.x}

[23] W. Kundig and S. Roseman. 1971. Sugar transport. I. Isolation of a phosphotransferase system from Escherichia coli. *Journal of Biological Chemistry* 246, 5 (1971), 1393–1406. https://www.scopus.com/inward/record.uri?eid=2-s2.0-0015217204&partnerID=40&md5=840beb714e55658f5d9514f3f94caa17 cited By 83.

[24] Michael T. Laub, Swaine L. Chen, Lucy Shapiro, and Harley H. McAdams. 2002. Genes directly controlled by CtrA, a master regulator of the Caulobacter cell cycle. *PROCEEDINGS OF THE NATIONAL ACADEMY OF SCIENCES OF THE UNITED STATES OF AMERICA* 99, 7 (APR 2 2002), 4632–4637. https://doi.org/{10.1073/pnas.062065699}

[25] Jae-Woo Lee, Young-Ha Park, and Yeong-Jae Seok. 2018. Rsd balances (p)ppGpp level by stimulating the hydrolase activity of SpoT during carbon source downshift in *Escherichia coli*. *PROCEEDINGS OF THE NATIONAL ACADEMY OF SCIENCES OF THE UNITED STATES OF AMERICA* 115, 29 (JUL 17 2018), E6845–E6854. https://doi.org/{10.1073/pnas.1722514115}

[26] Shenghua Li, Paul Brazhnik, Bruno Sobral, and John J. Tyson. 2009. Temporal Controls of the Asymmetric Cell Division Cycle in Caulobacter crescentus. *PLOS COMPUTATIONAL BIOLOGY* 5, 8 (AUG 2009). https://doi.org/{10.1371/journal.pcbi.1000463}

[27] Christian Lori, Shogo Ozaki, Samuel Steiner, Raphael Boehm, Sören Abel, Badri N. Dubey, Tilman Schirmer, Sebastian Hiller, and Urs Jenal. 2015. Cyclic di-GMP acts as a cell cycle oscillator to drive chromosome replication. *NATURE* 523, 7559 (JUL 9 2015), 236–U278. https://doi.org/{10.1038/nature14473}

[28] Norman D. Meadow, Roshan L. Mattoo, Regina S. Savtchenko, and Saul Roseman. 2005. Transient State Kinetics of Enzyme I of the Phosphoenolpyruvate:Glycose Phosphotransferase System of *Escherichia Coli*: Equilibrium and Second-Order Rate Constants for the Phosphotransfer Reactions with Phosphoenolpyruvate and HPr. *Biochemistry* 44, 38 (2005), 12790–12796. https://doi.org/10.1021/bi0502846

[29] Ralf Paul, Sören Abel, Paul Wassmann, Andreas Beck, Heiko Heerklotz, and Urs Jenal. 2007. Activation of the diguanylate cyclase PleD by phosphorylation-mediated dimerization. *JOURNAL OF BIOLOGICAL CHEMISTRY* 282, 40 (OCT 5 2007), 29170–29177. https://doi.org/{10.1074/jbc.M704702200}

[30] Ralf Paul, Tina Jaeger, SÃűren Abel, Irene Wiederkehr, Marc Folcher, Emanuele G. Biondi, Michael T. Laub, and Urs Jenal. 2008. Allosteric Regulation of Histidine Kinases by Their Cognate Response Regulator Determines Cell Fate. *Cell* 133, 3 (2008), 452 – 461. http://login.ezproxy.lib.vt.edu/login?url=http://search.ebscohost.com/login.aspx?direct=true&db=edselp&AN=S0092867408003954&site=eds-live&scope=site

[31] Katharina Pflüger and Víctor de Lorenzo. 2008. Evidence of In Vivo Cross Talk between the Nitrogen-Related and Fructose-Related Branches of the Carbohydrate Phosphotransferase System of *Pseudomonas putida*. *Journal of Bacteriology* 190, 9 (2008), 3374–3380. https://doi.org/10.1128/JB.02002-07 arXiv:https://jb.asm.org/content/190/9/3374.full.pdf

[32] Katharina Pflüger-Grau, Max Chavarría, and Víctor de Lorenzo. 2011. The interplay of the EIIA^{Ntr} component of the nitrogen-related phosphotransferase system (PTS^{Ntr}) of Pseudomonas putida with pyruvate dehydrogenase. *BIOCHIMICA ET BIOPHYSICA ACTA-GENERAL SUBJECTS* 1810, 10, SI (OCT 2011), 995–1005. https://doi.org/{10.1016/j.bbagen.2011.01.002}

[33] Tatyana L. Povolotsky and Regine Hengge. 2012. 'Life-style' control networks in *Escherichia coli*: Signaling by the second messenger c-di-GMP. *JIOCHIMICA OF BIOTECHNOLOGY* 160, 1-2 (JUL 31 2012), 10–16. https://doi.org/{10.1016/j.jbiotec.2011.12.024}

[34] Séverin Ronneau, Kenny Petit, Xavier De Bolle, and Régis Hallez. 2016. Phosphotransferase-dependent accumulation of (p)ppGpp in response to glutamine deprivation in *Caulobacter crescentus*. *NATURE COMMUNICATIONS* 7 (APR 2016). https://doi.org/{10.1038/ncomms11423}

[35] Kathleen R. Ryan, Ellen M. Judd, and Lucy Shapiro. 2002. The CtrA response regulator essential for Caulobacter crescentus cell-cycle progression requires a bipartite degradation signal for temporally controlled proteolysis. *JOURNAL OF MOLECULAR BIOLOGY* 324, 3 (NOV 29 2002), 443–455. https://doi.org/{10.1016/S0022-2836(02)01042-2}

[36] Ismael Sánchez-Osorio, Carlos A. Hernández-Martínez, and Agustino Martínez-Antonio. 2017. Modeling Asymmetric Cell Division in Caulobacter crescentus Using a Boolean Logic Approach. In *ASYMMETRIC CELL DIVISION IN DEVELOPMENT, DIFFERENTIATION AND CANCER*, Tassan, JP and Kubiak, JZ (Ed.). Results and Problems in Cell Differentiation, Vol. 61. 1–21. https://doi.org/{10.1007/978-3-319-53150-2_1}

[37] Moises Santillán. 2008. On the Use of the Hill Functions in Mathematical Models of Gene Regulatory Networks. *MATHEMATICAL MODELLING OF NATURAL PHENOMENA* 3, 2 (2008), 85–97. https://doi.org/{10.1051/mmnp:2008056}

[38] Olga Sarenko, Gisela Klauck, Franziska M. Wilke, Vanessa Pfiffer, Anja M. Richter, Susanne Herbst, Volkhard Kaever, and Regine Hengge. 2017. More than Enzymes That Make or Break Cyclic Di-GMP—Local Signaling in the Interactome of GGDEF/EAL Domain Proteins of Escherichia coli. *mBio* 8, 5 (2017). https://doi.org/10.1128/mBio.01639-17 arXiv:https://mbio.asm.org/content/8/5/e01639-17.full.pdf

[39] Tilman Schirmer and Urs Jenal. 2009. Structural and mechanistic determinants of c-di-GMP signalling. *NATURE REVIEWS MICROBIOLOGY* 7, 10 (OCT 2009), 724–735. https://doi.org/{10.1038/nrmicro2203}

[40] Xiling Shen, Justine Collier, David Dill, Lucy Shapiro, Mark Horowitz, and Harley H. McAdams. 2008. Architecture and inherent robustness of a bacterial cell-cycle control system. *PROCEEDINGS OF THE NATIONAL ACADEMY OF SCIENCES OF THE UNITED STATES OF AMERICA* 105, 32 (AUG 12 2008), 11340–11345. https://doi.org/{10.1073/pnas.0805258105}

[41] Stephen C. Smith, Kamal K. Joshi, Justin J. Zik, Katherine Trinh, Aron Kamajaya, Peter Chien, and Kathleen R. Ryan. 2014. Cell cycle-dependent adaptor complex for ClpXP-mediated proteolysis directly integrates phosphorylation and second messenger signals. *PROCEEDINGS OF THE NATIONAL ACADEMY OF SCIENCES OF THE UNITED STATES OF AMERICA* 111, 39 (SEP 30 2014), 14229–14234. https://doi.org/{10.1073/pnas.1407862111}

[42] Kartik Subramanian, Mark R. Paul, and John J. Tyson. 2013. Potential Role of a Bistable Histidine Kinase Switch in the Asymmetric Division Cycle of Caulobacter crescentus. *PLOS Computational Biology* 9, 9 (09 2013), 1–12. https://doi.org/10.1371/journal.pcbi.1003221

[43] I. Goryanin T. A. Karelina, H. Ma and O. V. Demin. 2011. EI of the Phosphotransferase System of *Escherichia coli*: Mathematical Modeling Approach to Analysis of Its Kinetic Properties. *Journal of Biophysics* 2011 (2011), 17 pages. https://doi.org/10.1155/2011/579402

[44] J. Wang, Ernst Dieter Gilles, Joseph W. Lengeler, and Knut Jahreis. 2001. Modeling of inducer exclusion and catabolite repression based on a PTS-dependent sucrose and non-PTS-dependent glycerol transport systems in *Escherichia coli* K-12 and its experimental verification. *Journal of Biotechnology* 92, 2 (2001), 133 – 158. https://doi.org/10.1016/S0168-1656(01)00354-6 Biochemical Engineering: Trends and Potentials.

[45] N. Weigel, M.A. Kukuruzinska, A. Nakazawa, E.B. Waygood, and S. Roseman. 1982. Sugar transport by the bacterial phosphotransferase system. Phosphoryl transfer reactions catalyzed by enzyme I of Salmonella typhimurium. *Journal of Biological Chemistry* 257, 23 (1982), 14477–14491. https://www.scopus.com/inward/record.uri?eid=2-s2.0-0020479946&partnerID=40&md5=b255ca19f8da4c11a7673e13aed0e0be cited By 94.

A SUPPLEMENTARY MATERIALS

A.1 Calculation for ODEs

A set of equations in Table 1 in the main text can be simplified further.

From Equation 8 and Equation 9, we can get the relationship between [EI] and [EI^{PEP}], as well as [EI~P] and [EI~P^{Pyr}]:

$$\begin{aligned} [\mathrm{EI}^{\mathrm{PEP}}] &= \frac{[\mathrm{PEP}][\mathrm{EI}]}{K_{b1}} \\ [\mathrm{EI}\sim\mathrm{P}^{\mathrm{Pyr}}] &= \frac{[\mathrm{Pyr}][\mathrm{EI}\sim\mathrm{P}]}{K_{b2}} \end{aligned} \tag{A.1}$$

We plug Equation A.1 and Equation 10 into Equation 5 and write the expression as follows:

$$\begin{aligned}\frac{d[\text{EI~P}]_{\text{tot}}}{dt} &= k_1 \times \frac{K_4+\epsilon[\text{Gln}]}{K_4+[\text{Gln}]} \times \frac{[\text{PEP}][\text{EI}]}{K_{b1}} - k_{-1}\frac{[\text{Pyr}][\text{EI~P}]}{K_{b2}} \\ &- k_2[\text{EI~P}][\text{NPr}] + k_{-2}[\text{NPr~P}][\text{EI}]\end{aligned} \tag{A.2}$$

Where $\text{EI} = \frac{[\text{EI}]_{\text{tot}} - [\text{EI~P}](1+\frac{[\text{Pyr}]}{K_{b2}})}{1+\frac{[\text{PEP}]}{K_{b1}}}$.

With the same method, we plug Equation 11 and Equation 12 into Equation 6 and Equation 7. Then we can rewrite ODEs A.2, 6, 7 as follows:

$$\begin{aligned}\frac{d[\text{EI~P}]_{\text{tot}}}{dt} &= k_1 \times \frac{K_4+\epsilon[\text{Gln}]}{K_4+[\text{Gln}]} \times \frac{[\text{PEP}][\text{EI}]}{K_{b1}} - k_{-1}\frac{[\text{Pyr}][\text{EI~P}]}{K_{b2}} \\ &- k_2[\text{EI~P}]([\text{NPr}]_{\text{tot}} - [\text{NPr~P}]) + k_{-2}[\text{NPr~P}][\text{EI}] \\ \frac{d[\text{NPr~P}]}{dt} &= k_2[\text{EI~P}]([\text{NPr}]_{\text{tot}} - [\text{NPr~P}]) \\ &- k_{-2}[\text{NPr~P}][\text{EI}] \\ &- k_3[\text{NPr~P}]([\text{EIIA}]_{\text{tot}} - \text{EIIA~P}]) \\ &+ k_{-3}([\text{NPr}]_{\text{tot}} - \text{NPr~P}])[\text{EIIA~P}] \\ \frac{d[\text{EIIA~P}]}{dt} &= k_3[\text{NPr~P}]([\text{EIIA}]_{\text{tot}} - \text{EIIA~P}]) \\ &- k_{-3}([\text{NPr}]_{\text{tot}} - \text{NPr~P}])[\text{EIIA~P}]\end{aligned} \tag{A.3}$$

Therefore, 7 ODEs and 5 algebraic equations in Table 1 can be rewritten into 7 ODEs:

$$\begin{aligned}\frac{d[(\text{p})\text{ppGpp}]}{dt} &= k_{\text{s.(p)ppGpp}} \times \text{SpoT}_{\text{sd}} \times \frac{[\text{GTP}]}{[\text{GTP}]+K_{\text{m3}}} \\ &- k_{\text{d.(p)ppGpp}} \times \text{SpoT}_{\text{hd}} \times \frac{[(\text{p})\text{ppGpp}]}{[(\text{p})\text{ppGpp}]+K_{\text{m4}}} \\ \frac{d[\text{cdG}]}{dt} &= k_{\text{s.cdG}} \times [\text{PleD}] \times \frac{K_1^2}{K_1^2+[\text{cdG}]^2} \times \frac{[\text{GTP}]^2}{[\text{GTP}]^2+K_{\text{m1}}^2} \\ &- k_{\text{d.cdG}} \times [\text{PdeA}] \times \frac{[\text{cdG}]}{[\text{cdG}]+K_{\text{m2}}} \\ \frac{d[\text{GTP}]}{dt} &= k_{\text{s.GTP}} \times [\text{GMP}] - k_{\text{d.GTP}} \times [\text{GTP}] - \frac{d[(\text{p})\text{ppGpp}]}{dt} \\ &- 2k_{\text{s.cdG}} \times [\text{PleD}] \times \frac{K_1^2}{K_1^2+[\text{cdG}]^2} \times \frac{[\text{GTP}]^2}{[\text{GTP}]^2+K_{\text{m1}}^2} \\ \frac{d[\text{GMP}]}{dt} &= 2k_{\text{d.cdG}} \times [\text{PdeA}] \times \frac{[\text{cdG}]}{[\text{cdG}]+K_{\text{m2}}} \\ &+ k_{\text{d.GTP}} \times [\text{GTP}] - k_{\text{s.GTP}} \times [\text{GMP}] \\ \frac{d[\text{EI~P}]_{\text{tot}}}{dt} &= k_1 \times \frac{K_3+\epsilon[\text{Gln}]}{K_3+[\text{Gln}]} \times \frac{[\text{PEP}][\text{EI}]}{K_{b1}} - k_{-1}\frac{[\text{Pyr}][\text{EI~P}]}{K_{b2}} \\ &- k_2[\text{EI~P}]([\text{NPr}]_{\text{tot}} - [\text{NPr~P}]) + k_{-2}[\text{NPr~P}][\text{EI}] \\ \frac{d[\text{NPr~P}]}{dt} &= k_2[\text{EI~P}]([\text{NPr}]_{\text{tot}} - [\text{NPr~P}]) \\ &- k_{-2}[\text{NPr~P}][\text{EI}] \\ &- k_3[\text{NPr~P}]([\text{EIIA}]_{\text{tot}} - \text{EIIA~P}]) \\ &+ k_{-3}([\text{NPr}]_{\text{tot}} - \text{NPr~P}])[\text{EIIA~P}] \\ \frac{d[\text{EIIA~P}]}{dt} &= k_3[\text{NPr~P}]([\text{EIIA}]_{\text{tot}} - \text{EIIA~P}]) \\ &- k_{-3}([\text{NPr}]_{\text{tot}} - \text{NPr~P}])[\text{EIIA~P}]\end{aligned} \tag{A.4}$$

The corresponding parameters are shown in Table 2 in main text.

A.2 Analysis of Weston's PleD~P simulation and current experimental PleD~P data

Whether a Caulobacter cell has a flagellum (swarmmer cell) or a holdfast (stalked cell) depends on the phosphorylation status of essential proteins, such as CtrA, DivK, and PleD[42]. The status of PleD is regulated by PleC-DivJ-DivK cell fate control system[30, 42]. Therefore, we can summarize how PleD~P behaves qualitatively during cell cycle (blue dot in Figure 1 in main text). PleD~P level starts to increase during swarmer-to-stalked transition (G1-TO-S transition) and keeps a relatively high level in stalked cell. Therefore, PleD~P is able to contribute to holdfast formation and CtrA proteolysis through synthesis of c-di-GMP.

Abel et al[2] have measured PleD~P quantitatively by Immunoblot. We used ImageJ to estimate the numeric level of PleD~P in the immunoblot (Figure A15). In Figure A15, PleD~P does not increase steadily. The dent around 40 min is in conflict with *C.crescentus*'s behavior during cell cycle. Compared with current numeric data we get from publications in literature, Weston's simulation (Figure 10(a) in main text) is more consistent with *C.crescentus*'s behavior. PleD~P keeps high in stalked cell and low in swarmer cell in his simulation. Therefore, we used his simulation of PleD~P instead of Abel et al's experimental data in our model.

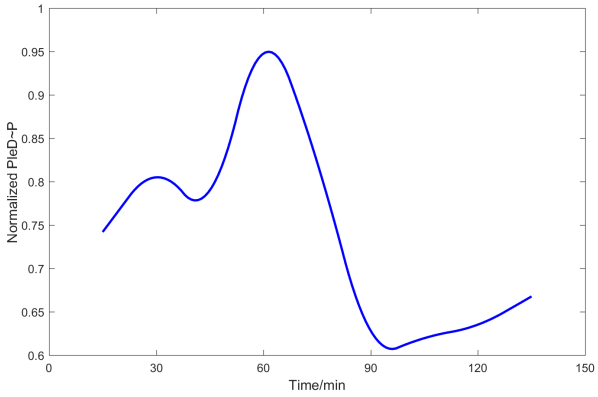

Figure A15: PleD~P extracted by ImageJ from Abel et al's[2] immunoblot. Abel et al's immunoblot of synchronized cultures of *Caulobacter crescentus* was stained with anti-PleD antibody. The cell undergoes swarmer-to-stalked transition around 30 min. Then the cell enters S-phase.